ACS OMEGA

Open Access

http://pubs.acs.org/journal/acsodf

Article

Synthesis and Characterization of Mg−Hydroxyapatite and Its β-Cyclodextrin Composite as Enhanced Bio-Carrier of 5-Fluorouracil Drug; Equilibrium and Release Kinetics

Mostafa R. Abukhadra,* Alaa T. Okasha, Sarah I. Al Othman, Haifa E. Alfassam, Noof A. Alenazi, Ali A. AlHammadi, and Ahmed A. Allam

Cite This: ACS Omega 2023, 8, 30247−30261

Read Online

ACCESS | Metrics & More | Article Recommendations

ABSTRACT: An advanced form of magnesium-doped hydroxyapatite (Mg·HAP) was integrated in composite with β-cyclodextrin producing a safe biocomposite (β-CD/HAP) as an enhanced delivery structure of traditional 5-fluorouracil (5-FU) chemotherapy during the treatment stages of colorectal cancer cells. The qualifications of β-CD/HAP as a carrier for 5-FU were followed based on the loading, release, and cytotoxicity as compared to Mg·HAP. β-CD/HAP composite exhibits notably higher 5-FU encapsulation capacity (272.3 mg/g) than Mg·HAP phase (164.9 mg/g). The 5-FU encapsulation processes into β-CD/HAP display the isotherm behavior of the Freundlich model (R^2 = 0.99) and kinetic assumptions of pseudo-first order kinetic (R^2 > 0.95). The steric studies reflect a strong increment in the quantities of the free sites after the β-CD integration steps (Nm = 61.2 mg/g) as compared to pure Mg·HAP (Nm = 42.4 mg/g). Also, the capacity of each site was enhanced to be loaded by 5 of 5-FU molecules (n = 4.45) in a vertical orientation. The 5-FU encapsulation energy into β-CD/HAP (<40 kJ/mol) reflects physical encapsulation reactions involving van der Waals forces and hydrogen bonding. The 5-FU release profiles of β-CD/HAP exhibit slow and controlled properties for about 80 h either in gastric fluid (pH 1.2) or in intestinal fluid (pH 7.4). The release kinetics and diffusion exponent (>0.45) signify non-Fickian transport and complex erosion/diffusion release mechanism. The free β-CD/HAP particles display a considerable cytotoxic effect on the HCT-116 cancer cells (33.62% cell viability) and its 5-FU-loaded product shows a strong cytotoxic effect (2.91% cell viability).

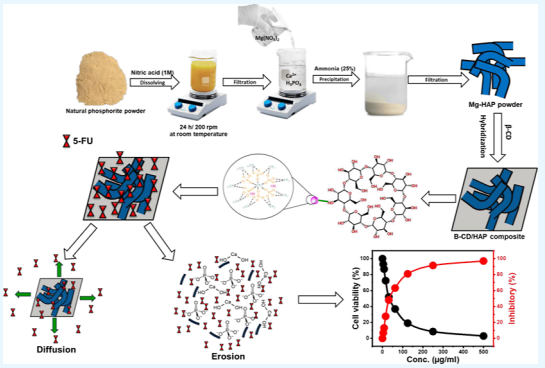

1. INTRODUCTION

Non-contagious diseases, particularly cancer, were responsible for roughly 72% of all recorded deaths worldwide, which is expected to rise to 75% within the coming next few years.[1,2] Colorectal cancer is a common malignant type of cancer that affects approximately 13% of cancer patients worldwide and represents one of the two major factors causing death and increasing the global death rate.[3−5] Colorectal cancer begins as a polyp within the mucosal layers and then spreads to the current submucosa and adjacent tissues. In the advanced stages of colorectal cancer, the formed neoplastic cells spread into the other nearby organs and lymph nodes.[6] Therefore, the production of effective and safe therapies that can inhibit significantly the tumor cells of colorectal cancer without detectable strong side effects represents a critical issue and hot research point of the international health authorities and the scientific communities.[5,7]

Various types of chemotherapies are widely used to conquer the continuous and progressive growth of cancer cells.[8,9] The mechanistic effect of the commonly tested chemotherapies includes the production of significant oxidative stress and effectively suppresses the DNA replication, resulting in the death of the infected malignant cells.[5,10] Regrettably, the majorities of the commonly used chemotherapies have toxic effects on normal cells and cause many serious side effects such as nausea, renal damage, and bone marrow suppression, especially with increasing the applied dosages.[11,12] As a result, some studies have been conducted to improve the existing species of conventional chemotherapies' safety, biological compatibility, therapeutic activity, and specificity.[12] This improvement has been suggested to be accomplished by the development of novel anticancer medications or by increasing the effectiveness and biological safety of the currently available conventional forms.[3]

Received: May 5, 2023
Accepted: July 25, 2023
Published: August 10, 2023

5-Fluorouracil (5-FU) is one of the most applied drugs as effective chemotherapy during the treatment of different species of tumor cells such as the rectum, breast, colorectal, and stomach cancers.[1,18] Unfortunately, among most of the used chemotherapies, the application of 5-FU is associated with several drawbacks that are related to its limited solubility, low selectivity, and high diffusion rate in addition to the reported significant toxic properties of its over dosages.[14,15] 5-FU exhibits strong toxic effects on the neural, gastrointestinal tract, cardiac, hematological, and dermatological reactions.[13,16] As a result, several advanced delivery systems were studied as effective methods to improve the therapeutic activity, curative value, solubility, release rate, and selectivity of 5-FU.[1,12,17] The effective encapsulation of the drug molecules into advanced biocompatible carriers was recommended strongly to regulate the delivered dosages along certain intervals and at controlled rates to avoid the commonly reported health drawbacks and expand the interaction duration.[18−21] Moreover, this can significantly enhance patient compliance and curative profiles in addition to its reduction effect on the degradation rate of the drug that preserves its concentration at the recommended level.[19,20]

In this regard, several inorganic, organic, and hybrid organic/inorganic structures such as mesoporous silica, zeolite, polymers, layered double hydroxide (LDH), CaO, and montmorillonites were evaluated as promising drug carriers for chemotherapies.[2,4,5,12,14] The previous materials demonstrated a significant effect in inducing the permeability and retention properties of the used drug.[4−6,9,18] Hydroxyapatite is a promising biomaterial species of the apatite family that exhibits $Ca_{10}(PO_4)_6(OH)_2$ and is widely used in numerous medical industries including tissue and bone engineering as well as effective drug delivery structure.[22−25] This was assigned to its significant chemical stability, surface area, acid−base adjustability, ion exchange capacity, long shelf life, flexible structure, and adsorption capacity.[26−28] As a biomaterial, it is bioactive, biodegradable, biocompatible, and osteoconductive without causing inflammation and toxicity.[8,29,30] However, the hydrophilic properties of its structure reduce its efficiency as carriers of the common drugs that are off organic chemical structure.[26,31] Consequently, many studies have been established to improve the physical, chemical, and biological properties of HAP by controlling its morphology, chemical composition, and crystallite size in addition to its surface functionalization and hybridization by polymers and other active chemical groups.[26,32,33] The hybrid composites of HAP and the reactive natural or synthetic polymers can successfully overcome the reported drawbacks during the application of it as a delivery system including the low encapsulation capacity, uncontrollable release rate, high brittleness, easy agglomeration, and poor plasticity.[16,25]

β-Cyclodextrin (β-CD) is a unique and important biocompound that has received much research attention as an essential component in a variety of hybrids with various types of inorganic materials for both medicinal and environmental industries.[1,34] This was primarily attributed to its accessibility, biological compatibility, stable chemical composition, notable adsorption, and non-toxic qualities.[35,36] On a chemical basis, β-CD demonstrates a cyclic glucopyranose framework that is built up of 6 or 7 glucose subunits that are joined or linked to each other by different forms of α (1 → 4) glycosidic bond.[34,37] While the outside surfaces of these units and corresponding chemical groups show substantial polarity, the interior frameworks of β-CD possess hydrophobic characteristics.[38] This promotes its incorporation into hybrid materials with inorganic components and the drug-loading capabilities of synthetic carriers depending on their physicochemical characteristics.[35,39] The β-CD considerably increases the drug's physicochemical qualities, including its solubility in water, chemical resistance, therapeutic activity, and durability.[40]

Therefore, the present study aims to develop a magnesium-bearing hydroxyapatite (Mg·HAP)-based composite with β-cyclodextrin (β-CD) as a multifunctional structure (β-CD/HAP) with significantly improved physicochemical, biologically compatible, and antitumor characteristics during its evaluation as a cheap and reliable carrier of 5-fluorouracil medication (5-FU). For the first time, encapsulating behaviors, releasing profiles, and cytotoxic influences on colorectal cancer cells (HCT-116) have been investigated to assess the characteristics of Mg·HAP and its composite with β-CD (β-CD/HAP) as prospective carriers of 5-FU molecules. Additionally, based on kinetic and equilibrium investigations, the controlling mechanisms throughout the encapsulation and release stages were emphasized.

2. RESULTS AND DISCUSSION

2.1. Characterization of the Carrier. *2.1.1. XRD Analysis.* The XRD patterns reflected the structure effect of the integration procedures on the individual components (Figure 1). The recognized diffraction pattern of Mg·HAP

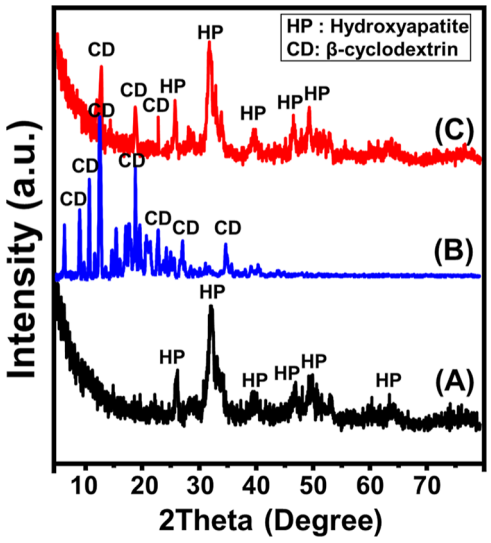

Figure 1. XRD pattern of synthetic magnesium hydroxyapatite (Mg·HAP) (A), β-cyclodextrin (B), and synthetic β-CD/HAP (C).

reflects the successful synthesis of hydroxyapatite with an average crystallite size of 11.8 nm. The identification peaks of Mg·HAP was detected at 26.28 (002), 28.63 (210), 32.29 (211), 40 (310), 47.1 (222), 50.29 (213), 53.55 (004), and 64.28° (304) (JCPSD 00-001-1008) (Figure 1). The remarkable upshifting of these peaks as compared to the reference pattern of hydroxyapatite was assigned to the structural impact of the doped Mg^{2+}.[32,42] The recognized pattern of the incorporated β-cyclodextrin polymer during the production of the composite display strong crystalline nature and show several intensive diffraction peaks [6.80 (001), 9.20 (101), 10.83 (011), 12.57 (041), 13.0 (070), 15.55 (141),

https://doi.org/10.1021/acsomega.3c02982
ACS Omega 2023, 8, 30247−30261

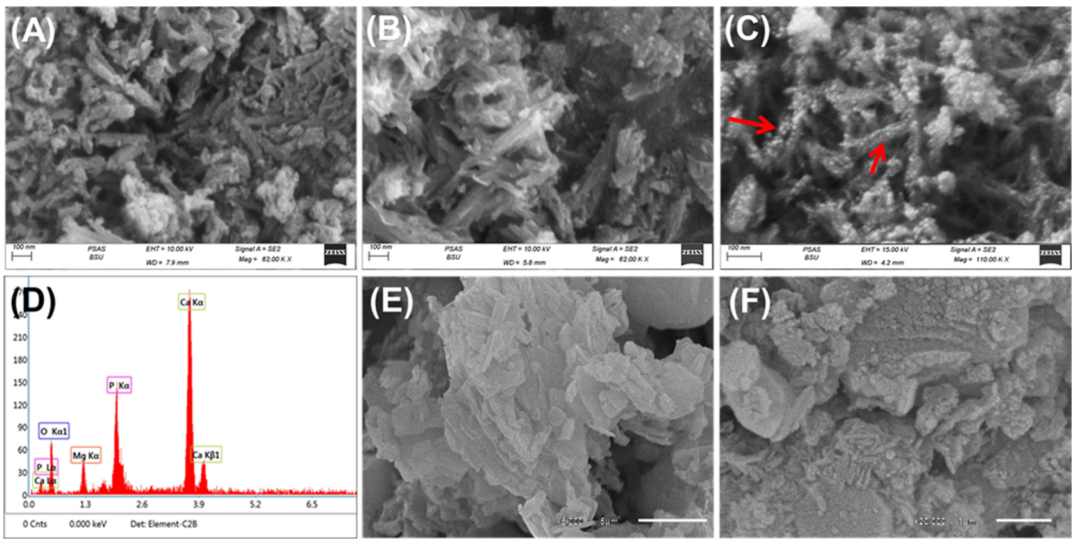

Figure 2. SEM images of the synthetic magnesium hydroxyapatite (Mg·HAP) (A−C), EDX spectrum of the synthetic M·HAP (D), and SEM images of the synthetic β-CD/HAP (E,F).

18.90 (230), 19.80 (091), 21.90 (042), 23.00 (251), 25.81 (162), 27.34 (222), and 34.90° (223)] (Figure 1B). The observed pattern of β-CD/HAP demonstrates the existence of the diffraction peaks of hydroxyapatite in addition to the integrated β-cyclodextrin but at notably deviated positions. This pattern demonstrates the formation of the composite between Mg·HAP and β-cyclodextrin might be involved in grafting of the β-CD chains, formation of chemical complexes, or hydrogen bonding.

2.1.2. SEM. The synthetic Mg·HAP was detected as needle-like or fibrous-like nanoparticles that connected with each other forming branches or bundles (Figure 2A). The random orientation of the Mg·HAP bundles in addition to their intersection resulted in a porous matrix in addition to the structural porosity of Mg·HAP (Figure 2B). The high SEM magnification image of the Mg·HAP bundles displayed the decoration of the particles with numerous nano-dots (Figure 2C). The synthetic Mg·HAP bundles display a 20 to 60 nm average diameter and 50 to 250 nm as average length. Whereas fibrous particles of the bundles exhibit an average diameter from 2 to 10 nm and an average length between 20 and >100 nm. Moreover, the EDX spectrum of the detected bundles reflected its composition as magnesium-rich hydroxyapatite (Ca, P, Mg, and O) (Figure 2D). Regarding the observed SEM images of the synthetic β-CD/HAP, the synthetic particles demonstrate significant orientation and entrapment of the Mg·HAP grains within the matrix of β-CD produce agglomerated particles with significantly different morphologies (Figure 2E,F). Moreover, the Mg·HAP grains disseminated randomly within the integrated β-CD producing irregular surface and rugged topography that can enhance the surface area and the exposure interface. Additionally, there is a notable intersection either between the β-CD chains or between the Mg·HAP and β-CD that leads to the formation of a network of bent platelets or lenticular-like grains (Figure 2E,F). Additionally, the textural properties reflected a significant effect of the described morphological features on the porosity and surface area of the composite. The determined surface area of Mg·HPA (93.7 m^2/g) is enhanced at a considerable rate after the incorporation of β-CD chains to be 95.2 m^2/g.

2.1.3. FT-IR Spectroscopy. The FT-IR spectra of Mg·HPA, β-CD, β-CD/HAP, and 5-FU encapsulated β-CD/HAP were evaluated to follow the expected changes in the essential chemical groups during the synthesis of the composite and loading of the drug (Figure 3). The essential functional groups

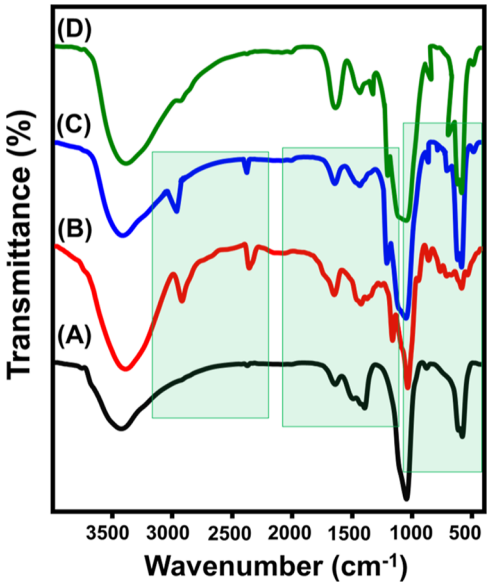

Figure 3. FT-IR spectra of synthetic magnesium hydroxyapatite (Mg·HAP) (A), β-cyclodextrin (B), synthetic β-CD/HAP (C), and 5-FU encapsulated β-CD/HAP (D).

of hydroxyapatite were identified clearly from the spectrum of Mg·HPA. This involved the essential phosphorus-bearing chemical groups such as asymmetric P−O bonds of the PO_4^{3-} group (1039.4 cm^{-1}), HPO_4^{2-} groups (871.2 cm^{-1}), symmetric (570.8 cm^{-1}) and asymmetric (603.3 cm^{-1}) O−P−O bonds of the PO_4^{3-} groups, in addition to the hydroxyl groups (O−H) (3434.4 cm^{-1}) (Figure 3A).[26,32,43,44] The corresponding bands of N−H bonds (1390.6 cm^{-1}) and CO_3^{2-} groups (2376.19 cm^{-1}) were assigned to the trapped ions during the dissolution of the precursor by nitric acid and the evolved CO_2 gas from the dissolved carbonate impurities,

https://doi.org/10.1021/acsomega.3c02982
ACS Omega 2023, 8, 30247−30261

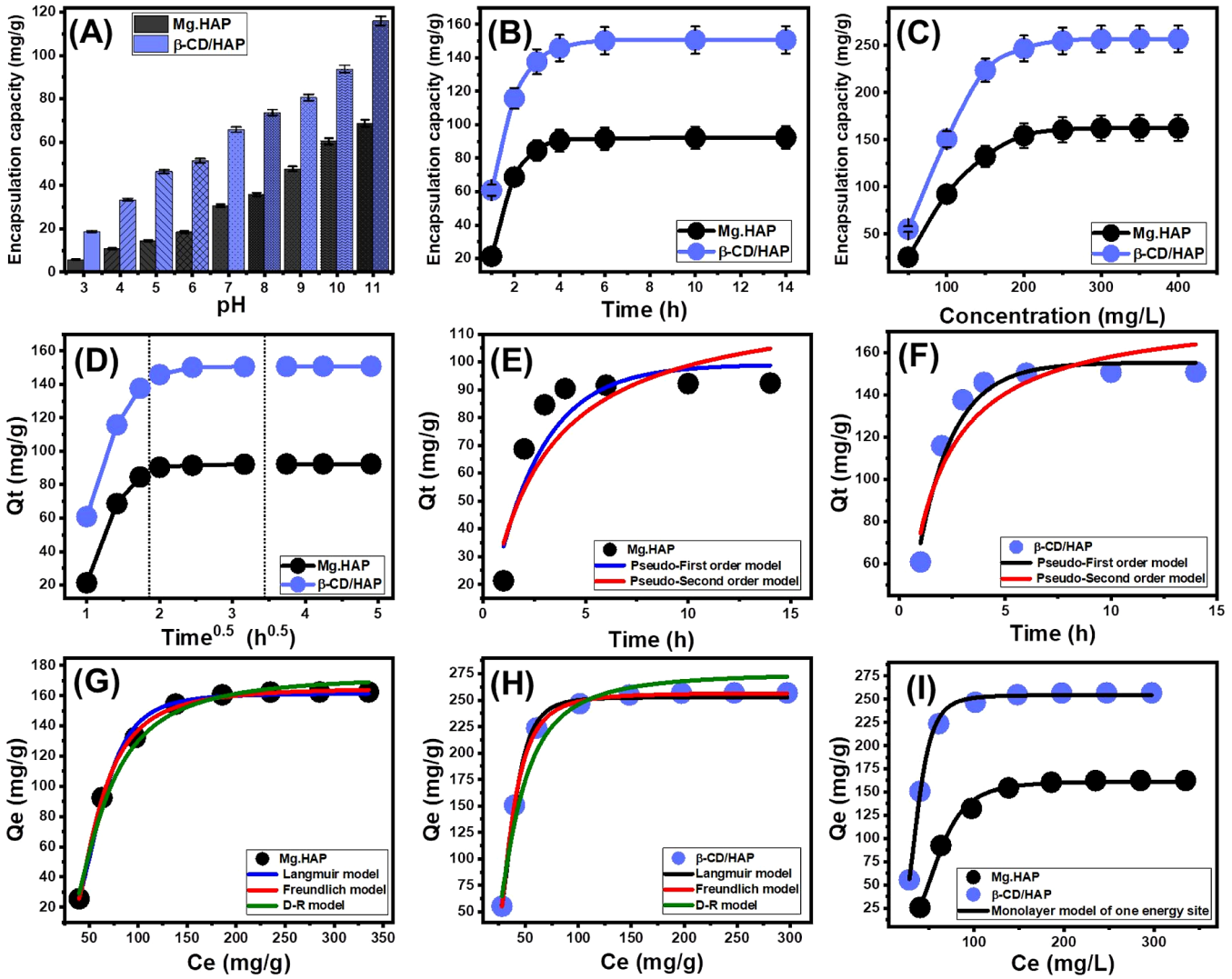

Figure 4. Effect of the solution's pH on the encapsulation of 5-FU (A), effect of encapsulation duration on the capacities of Mg·HAP and *β*-CD/HAP (B), effect of 5-FU initial concentration on the capacities of Mg·HAP and *β*-CD/HAP (C), intra-particle diffusion curves of 5-FU encapsulation results by Mg·HAP and *β*-CD/HAP (D), fitting of the 5-FU encapsulation process with the kinetic models (E,F), fitting of the 5-FU encapsulation process with the classic isotherm models (G,H), and fitting of the 5-FU encapsulation process with advanced isotherm model (monolayer model of one energy) (I).

respectively (Figure 3A).[41,45,46] For the free *β*-cyclodextrin, its spectrum reflects notably the characteristic groups of the polymeric polysaccharide structures such as O−H stretching vibration (3376 cm^{-1}), −CH/CH_2 asymmetrical stretching (2926 cm^{-1}), stretching mode of C−C and/or H−O−H deformation within the *β*-CD cavity (1666.2 cm^{-1}), C═O stretching and/or OH bending (1636 cm^{-1}), C−OH bending vibration (1482 cm^{-1}), symmetrical C−O−C (1200 cm^{-1}), asymmetrical C−O−C stretching (1158 cm^{-1}), and symmetrical C−O stretching (1000 cm^{-1}) (Figure 3B).[36,39]

The successful synthesis of *β*-CD/Mg·HPA composite can be detected notably during the inspection of its FT-IR spectrum (Figure 3C). The main groups of Mg·HPA [3424 cm^{-1} (OH stretching), 1040 cm^{-1} (P−O stretching vibration for PO_4^{3-}), and 571.6 (P−O bending vibration for PO_4^{3-})] were observed in complex with *β*-CD [asymmetric −CH/CH_2 (2905 cm^{-1}), C−C (1663.2 cm^{-1}), C−OH bending (1468.3 cm^{-1}), and symmetrical C−O−C (1211.6 cm^{-1})] (Figure 3C). The detection of both the organic and inorganic chemical groups that are related to the two components of the composite, in addition to the marked fluctuation in the essential absorption bands, validates the significant formation of the composite with remarkable interaction between the active chemical groups of its components. For the obtained spectrum of the *β*-CD/Mg·HPA after its loading with 5-FU molecules, the observable deviation in the main bands in addition to marked identification bands of 5-FU chemical structure [CF═CH (775.12 cm^{-1})] confirms the trapping of the drug ions within the structure of the composite[4,14] (Figure 3D).

2.2. Encapsulation of 5-FU Drug. *2.2.1. Influence of the Encapsulation Parameters. 2.2.1.1. Effect of pH.* The effect of the pH of the solutions on the loading capacities of Mg·HAP and *β*-CD/HAP was tested in a range of pH 3 to 11 at different levels for the other factors that could affect the results [dose: 20 mg; 5-FU concentration: 100 mg/L; temperature: 20 °C; volume: 50 mL; time: 2 h]. High pH conditions have been verified to significantly improve the encapsulation properties of 5-FU into Mg·HAP and *β*-CD/HAP (Figure 4A). This is detectable from pH 3 [Mg·HAP (5.8 mg/g) and *β*-CD/HAP

https://doi.org/10.1021/acsomega.3c02982
ACS Omega 2023, 8, 30247−30261

Table 1. Obtained Fitting Theoretical Parameters of the Studied Kinetic, Classic Equilibrium, Advanced Equilibrium, Van't Hoff Equation, and Release Kinetic Models

model	parameters	Mg·HAP	β-CD/HAP
	Kinetic Models		
pseudo-first-order	K_1 (min^{-1})	0.415	0.597
	$Q_{e(Cal)}$ (mg/g)	99.0	155.1
	R^2	0.88	0.96
	X^2	2.75	0.54
pseudo-second-order	k_2 (g $mg^{-1}min^{-1}$)	0.0031	0.0038
	$Q_{e(Cal)}$ (mg/g)	124.0	180.4
	R^2	0.83	0.89
	X^2	4.01	1.68
	Isotherm Models		
Langmuir	$Q_{max\ (mg/g)}$	166.4	267.4
	b (L/mg)	1.17×10^{-7}	8.61×10^{-8}
	R^2	0.99	0.99
	X^2	0.146	0.104
	R_L	0.99	0.99
Freundlich	$1/n$	0.36	0.30
	k_F (mg/g)	165.1	256.6
	R^2	0.99	0.99
	X^2	0.027	0.01
D−R model	β (mol^2/kJ^2)	0.02897	0.01165
	Q_m (mg/g)	173.28	275.8
	R^2	0.99	0.97
	X^2	0.31	1.67
	E (kJ/mol)	4.15	6.55
monolayer model of one energy	n	3.89	4.45
	Nm (mg/g)	42.4	61.2
	$Q_{(sat)}$ (mg/g)	164.9	272.3
	ΔE (kJ/mol)	−7.54	−8.13
	Thermodynamics		
$\Delta G°$ (kJ mol^{-1})	293.13	−12.83	−14.24
	303.13	−13.14	−14.64
	313.13	−13.30	−15.04
	323.13	−13.27	−15.33
$\Delta H°$ (kJ mol^{-1})		−8.31	−4.23
$\Delta S°$ (J K^{-1} mol^{-1})		15.65	34.3

	release kinetics			
	determination coefficient			
	Mg·HAP		β-CD/HAP	
models	gastric fluid (pH 1.2)	intestinal fluid (pH 7.4)	gastric fluid (pH 1.2)	intestinal fluid (pH 7.4)
zero-order	0.78	0.89	0.90	0.80
first order	0.93	0.96	0.93	0.98
Higuchi	0.92	0.97	0.98	0.94
Hixson−Crowell	0.99	0.98	0.99	0.99
Korsmeyer−Peppas	0.95	0.98	0.95	0.96
n	0.64	0.73	0.64	0.64

(18.5 mg/g)] to pH 11 [Mg·HAP (68.7 mg/g) and β-CD/HAP (115.8 mg/g)] (Figure 4A). Therefore, it was advised to load 5-FU into Mg·HAP and β-CD/HAP via encapsulation procedures at basic pH levels. Generally, the adjusted pH of the solutions influences the ionization properties of 5-FU as well as the dominant surficial charges of Mg·HAP and β-CD/HAP. The chemical structure of the 5-FU medication demonstrates substantial ionization characteristics at higher pH conditions (alkaline) in contrast to its characteristics in acidic to neutral circumstances.[5,12] The 5-FU ions' mobility, diffusion, and interactions with the activated and free-loading sites of Mg·HAP and β-CD/HAP are strongly influenced by the rise in ionization degrees, which enhance the loading capacities at the basic solutions. Additionally, the expected dissolution of the hydroxyapatite structure within the acidic condition adversely affects the loading capacity of both Mg·HAP and β-CD/HAP.[16]

2.2.1.2. Encapsulation Duration. The effect of encapsulating duration on the attained capacities of Mg·HAP and β-CD/HAP was examined experimentally in a period ranging from 1 to 14 h, alongside the other influencing variables held constant [5-FU concentration: dosage: 20 mg; 100 mg/L; pH: 11; temperature: 20 °C; volume: 50 mL]. The 5-FU encapsulating performances of Mg·HAP and β-CD/HAP show noteworthy

https://doi.org/10.1021/acsomega.3c02982
ACS Omega 2023, 8, 30247−30261

improvement in terms of both encapsulating rates and loading amounts in mg/g with systematic extension for the assessed time period (Figure 4B). This improvement effect appears from 1 to 6 h; beyond that, the increase in testing duration has little to no effect on the observed loading rate or the amounts of 5-FU that were encapsulated, and the graphs show stability states of almost steady values (Figure 4B). Such characteristics represent the equilibration stages of the encapsulation processes of Mg·HAP and β-CD/HAP [Mg·HAP (92.4 mg/g) and β-CD/HAP (150.7 mg/g)]. The rapid loading rates that were observed and the sudden rise in the 5-FU encapsulated amounts have been attributed to the presence of numerous active encapsulating sites in their free forms on Mg·HAP and β-CD/HAP during the beginning of the processes.[47] With increasing test periods, 5-FU is gradually encapsulated into the Mg·HAP and β-CD/HAP-free sites, causing occupancy and consumption of them that sharply reduces their availability. As a result, the 5-FU encapsulating rate significantly decreased after a set period of time, and the Mg·HAP and β-CD/HAP particulates exhibited slight improvements in 5-FU loading capabilities. Following full occupancy of all available sites by the loaded 5-FU molecules, the equilibration statuses of Mg·HAP and β-CD/HAP were established.[48]

2.2.1.3. 5-FU Concentration. The actual influence of the assessed 5-FU concentration on the proved loading characteristics of Mg·HAP and β-CD/HAP was monitored throughout an examined range of 50 to 700 mg/L at adjusting values of all other variables that affected it [duration: 14 h; pH: 11; dosage: 20 mg; volume: 50 mL; temperature: 20 °C]. The maximal capacities of Mg·HAP and β-CD/HAP besides their equilibrium characteristics, depend extensively on the starting 5-FU concentrations as an operational factor throughout the loading procedures. In the presence of high starting concentrations of 5-FU, the amounts of 5-FU encapsulated within Mg·HAP and β-CD/HAP significantly increased (Figure 4C). High levels of 5-FU in a given volume have a strong accelerating effect on the ions' transfer and mobility, which increases the likelihood of collisions besides the chemical interactions that exist between the active centers of Mg·HAP and β-CD/HAP particulates and the dissolved molecules of drugs.[38,49] As a result, Mg·HAP and β-CD/HAP become more effective in encapsulating 5-FU up to a specific concentration (250 mg/L) (Figure 4C). Once these levels were tested, a rise in the assessed 5-FU concentration had no effect on the amounts of 5-FU that were encapsulated, which typically indicate the equilibrium loading conditions of Mg·HAP and β-CD/HAP to be potential carriers (Figure 4C). As a result, Mg·HAP and β-CD/HAP both reach their maximal 5-FU encapsulating capabilities [162.4 mg/g (Mg·HAP) and 256.8 mg/g (β-CD/HAP)]. The substantially greater 5-FU encapsulating capacity of β-CD/HAP was attributed to a number of factors, including (1) the observed rise in surface area following the β-CD incorporation step, (2) the organophilic characteristics of the β-CD/HAP, as in comparison with a hydrophilic Mg·HAP that promote its affinity toward the dissolved organic molecules that form 5-FU, and (3) a noticeable rise in the total number of available functional encapsulation sites.

2.2.2. Encapsulation Mechanism. 2.2.2.1. Kinetic Studies. Intra-particle diffusion properties: The processes that load 5-FU into Mg·HAP and β-CD/HAP exhibit intra-particle diffusion curves with segment-like properties, comprising three discrete phases with no crossovers with the beginning points of these curves (Figure 4D). This demonstrates the 5-FU loading through collaborative mechanisms as well as the significant influence of drug ion diffusion in the direction of the reactive surfaces of Mg·HAP and β-CD/HAP.[49,50] This may comprise (A) loading processes by the surficial or exterior active sites (border), (B) mechanistic effects of intra-particle diffusion processes, and (C) the effect of the attended equilibration or saturation states.[51] The existence of the first step in the curves implies that exterior loading mechanisms were active and dominant as the investigation began, and the total number of the existing exterior sites strongly controls the 5-FU loading rates (Figure 4D).[52] By prolonging the time, another stage (Figure 4D) has been observed that indicates the presence of different regulating mechanisms, including the influence of the layered loading operations and the 5-FU diffusion reactions.[51,53] Finally, the third stage was recognized as the dominant phase during the equilibrium states of Mg·HAP and β-CD/HAP. This demonstrates that the loaded 5-FU ions have occupied or consumed all of the functional binding sites (Figure 4D).[26,49] In this stage, several types of processes, including molecular attraction and/or interionic attraction, can direct the loading behaviors.[38]

Kinetic modeling: Based on the kinetic hypotheses of the two different models, the pseudo-first order model (P.F.) (eq 1) and the pseudo-second order (P.S.) (eq 2) model, the kinetic characteristics of the 5-FU encapsulation process into Mg·HAP (Figure 4E) and β-CD/HAP (Figure 4F) have been illustrated. The level of agreement between the loading behaviors and the kinetic assumptions of the two models was evaluated by means of non-linear fitting with their descriptive equations, with the correlation coefficient (R^2) and chi-square (χ^2) as key markers of the fitting degree (Table 1; Figure 4E,F).

$$Q_t = Q_e(1 - e^{-k_1 \cdot t}) \quad (1)$$

$$Q_t = \frac{Q_e^2 k_2 t}{1 + Q_e k_2 t} \quad (2)$$

The determined values of R^2 and χ^2 show that the P.F. model's kinetic characteristics more appropriately represent the 5-Fu loading processes into the Mg·HAP and β-CD/HAP than the P.S. model. The striking match between formerly identified equilibrium capacities experimentally [Mg·HAP (92.4 mg/g) and β-CD/HAP (150.7 mg/g)] and theoretically estimated values from the P.F. model as fitting parameters [Mg·HAP (99.0 mg/g) and β-CD/HAP (155.1 mg/g)] (Table 1) provided further validation for these fitting results. Based on the kinetic characteristics of the representative P.F. model, the loading of 5-Fu into Mg·HAP and β-CD/HAP proceeded primarily by physical processes that may have entailed van der Waals forces and/or electrostatic attractions.[54,55] However, the loading processes are better described by the P.F. model than by the P.S. model, the fitting findings are still in substantial agreement with the P.S. model. Consequently, it was anticipated that there would be a minor impact or assisting influence for weak chemical reactions such as hydrogen bonding, electron sharing, hydrophobic interactions, and chemical complexes during the loading of 5-FU into Mg·HAP and β-CD/HAP.[49,54] The collaboration of both physical and chemical processes entailed the production of a chemically

https://doi.org/10.1021/acsomega.3c02982
ACS Omega 2023, 8, 30247−30261

loaded layer of the medication, followed by the construction of a physically loaded layer utilizing the first layer as a substrate.[56]

2.2.2.2. Equilibrium Studies. Classic isotherm modeling: The equilibrium properties of the 5-FU loading processes into Mg·HAP and β-CD/HAP as prospective carriers have been described utilizing the Langmuir (eq 3) and Freundlich (eq 4) assumptions, as well as the Dubinin−Radushkevich (D−R) (eq 5) hypotheses. The models' illustrative equations were used to non-linearly fit the findings, and the degree of fit was measured by the value of the correlation coefficient (R^2) and chi-squared (χ^2) [Table 1; Figure 4G (Mg·HAP), and H (β-CD/HAP)].

$$Q_e = \frac{Q_{max} b C_e}{(1 + bC_e)} \tag{3}$$

$$Q_e = K_f C_e^{1/n} \tag{4}$$

$$Q_e = Q_m\, e^{-\beta\varepsilon^2} \tag{5}$$

The detected values of R^2 and χ^2 indicate slightly higher fitting of the 5-FU encapsulation processes into both Mg·HAP and β-CD/HAP with the equilibrium hypothesis of the Freundlich model than the Langmuir model. This concordance with the isotherm of Freundlich model implies that the encapsulation has occurred heterogeneously into the Mg·HAP and β-CD/HAP particles in multilayer forms.[54,55] Furthermore, the determined RL parameter of the 5-FU encapsulating process has a value smaller than unity, which is generally a sign of the favorable characteristics of the loading reactions.[26,52] The anticipated maximal 5-FU encapsulating capacities (Q_{max}) were calculated as a theoretical parameter based on the isotherm analysis of Langmuir model. The Q_{max} of Mg·HAP and β-CD/HAP are 166.4 and 267.4 mg/g, respectively.

Regardless of whether the surfaces of Mg·HAP and β-CD/HAP are homogeneous or heterogeneous, the isothermal characteristics of the examined D−R model may provide insight into the energetic heterogeneity of these potential carriers of 5-FU.[57] The predominant loading mechanisms, whether chemical or physical in type, are highlighted by the Gaussian energy (E), which has been determined as an obtainable mathematical parameter of the D−R model. The E values of the chemical mechanisms are more than 16 kJ/mol, but those of the physical mechanisms are less than 8 kJ/mol. Gaussian energy levels from 8 to 16 kJ/mol indicate complex processes (physical and chemical) or weak chemical loading processes.[26,57] The 5-FU loading activities of Mg·HAP and β-CD/HAP had Gaussian energies of 4.15 and 6.55 kJ/mol, respectively (Table 1). The findings indicated that, in addition to the hypothesized influence of ion exchange mechanisms (0.6 to 25 kJ/mol), the physical process that occurred during the loading of 5-FU had a major impact.

Advanced isotherm models: The designated advanced isotherm mathematical models, based on the equilibrium fundamentals of statistical physics theory, give further insight into Mg·HAP and β-CD/HAP as 5-FU carriers with regard to the carrier surfaces/drug solution interface. The loading behaviors and their controllable mechanistic activities were studied via an advanced monolayer model with one energy (eq 6) and its related theoretical parameters, either steric or energetic (Figure 4I; Table 1). The determination coefficients (R^2) and the root mean square error (RMSE) were determined to be the main factors that determine the fitting degrees

$$Q = nN_o = \frac{nN_M}{1 + \left(\frac{C_{1/2}}{C_e}\right)^n} = \frac{Q_o}{1 + \left(\frac{C_{1/2}}{C_e}\right)^n} \tag{6}$$

The mathematically investigated steric parameters that were derived from the model comprised the density of the occupied active loading sites ($Nm_{(5\text{-FU})}$) of Mg·HAP and B-CD/HAP, the number of loaded 5-Fu ions per one active site ($n_{(5\text{-FU})}$), and the 5-Fu loading capacities of Mg·HAP and B-CD/HAP at their saturation levels ($Q_{sat(5\text{-FU})}$) (Table 1). The determined 5-FU loading energy (E) was the evaluated energetic parameter (Table 1). In accordance with the steric parameters, the formation of β-CD/HAP composite resulted in notable enhancement in its qualification as a potential carrier of 5-FU as compared to the pure phase. After the incorporation of β-CD, the total amount of the functional active sites during the process of 5-FU encapsulation significantly increased [$Nm_{(5\text{-FU})}$ = 42.4 mg/g (Mg·HAP) and 61.2 mg/g (β-CD/HAP)], which might be explained by the incorporation of additional active functional groups that are related to the β-CD or by the improvement of the interactive interface due to the significant enhancement in surface area (Table 1). The significantly higher $Nm_{(5\text{-FU})}$ of β-CD/HAP induced strongly its loading capacity especially during its saturation state to be 272.3 mg/g in comparison with 164.9 mg/g for Mg·HAP. The numbers of the entrapped 5-FU ions per each single free site of Mg·HAP and β-CD/HAP [$n_{(5\text{-FU})}$ = 3.89 (Mg·HAP) and 4.45 (β-CD/HAP)] are >1 indicating that the loaded ions are oriented vertically and are encapsulated by multi-molecular mechanisms (Table 1).[58,59]

The energies of the 5-FU encapsulation processes (ΔE) into Mg·HAP and β-CD/HAP were determined based on eq 7 considering 5-FU rest concentration at the half saturations of Mg·HAP and β-CD/HAP ($C_{1/2}$) and the determined absolute solubility of 5-FU (Table 1).

$$\Delta E = -RT \ln\left(\frac{S}{C_{1/2}}\right) \tag{7}$$

The determined loading energies of 5-FU into Mg·HAP and β-CD/HAP are −7.54 and −8.13 kJ/mol, respectively. These values support the previous findings about the physical and weak chemical encapsulation mechanisms ($\Delta E \leq 40$ kJ/mol) of 5-FU into Mg·HAP and β-CD/HAP.[60,61] These processes might involve van der Waals forces (ΔE = 4 to 10 kJ/mol), dipole forces (ΔE = 2 to 29 kJ/mol), and hydrogen bonding (ΔE < 30 kJ/mol). This might involve electrostatic attractions and hydrogen bonding between the 5-FU amino groups and hydroxyl groups of hydroxyapatite and β-CD structure.

2.2.2.3. Thermodynamic Studies. The thermodynamic characteristics of the 5-FU encapsulating processes by Mg·HAP and β-CD/HAP were assessed considering certain values for the other influencing factors (duration: 14 h; pH: 11; dosage: 20 mg; volume: 50 mL; and concentration: 400 mg/L) over tested temperatures that ranged from 20 to 60 °C. The thermodynamic characteristics, which included key functions like Gibbs free energy ($\Delta G°$) (eq 8) as well as entropy ($\Delta S°$) and enthalpy ($\Delta H°$) were obtained as parameters via the linear regression analysis with the Van't Hof formula (eq 9) (Figure 5).[14]

$$\ln(K_c) = \frac{\Delta S°}{R} - \frac{\Delta H°}{RT} \tag{8}$$

https://doi.org/10.1021/acsomega.3c02982
ACS Omega 2023, 8, 30247−30261

$$\Delta G^{\circ} = -RT \ln K_c \quad (9)$$

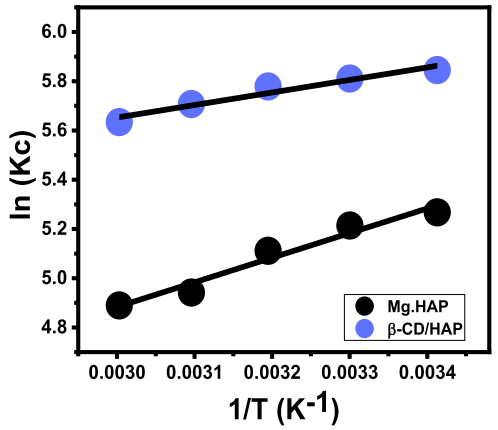

Figure 5. Fitting of the 5-FU encapsulation results with Van't Hof thermodynamic equation.

The detection of ΔG° and ΔH° parameters as negative values signifies the spontaneous behavior of these loading processes in addition to their exothermic and favorable properties either by Mg·HAP or β-CD/HAP (Table 1). Furthermore, the determination of ΔS° parameter as positive values either by Mg·HAP or β-CD/HAP validates the significant enhancement in the randomness properties of the loading systems as chemical reactions with the regular rise in the evaluated temperature.

2.3. In Vitro Release Profiles. The release profiles of Mg·HAP and β-CD/HAP were analyzed by measuring the percentages of 5-FU molecules that moved through gastric fluid (pH 1.2) and intestinal fluid (pH 7.4), which were used to simulate the conditions of cancerous cells (Figure 6). The observed 5-FU diffusion percentages from Mg·HAP and β-CD/HAP with the two investigated buffers endorse noticeable variations in the recognized rates with a considerable increase in the estimated release durations (Figure 6A,B). The 5-FU release rates from Mg·HAP and β-CD/HAP display quick characteristics that correlate to significant changes in the measured 5-Fu released quantities. After specific release periods, the detectable 5-FU diffusion rates significantly decreased, and no appreciable improvement in the released quantities could be observed (Figure 6). By this time, the release reactions of Mg·HAP and β-CD/HAP had subsequently stabilized. The quick 5-FU diffusion properties that were observed during the earliest release periods were attributed to the sudden desorption of the poorly bonded as well as physically loaded 5-FU ions on the surficial loading sites of Mg·HAP and β-CD/HAP.[62−64] Following full desorption of such barely bonded and surficially loaded 5-FU ions, their release characteristics were controlled by the strongly bonded ions or those formed chemical complexes, as well as the entrapped 5-Fu ions inside the structural pores of Mg·HAP and β-CD/HAP, which negatively influenced the observed diffusion rates (Figure 6A,B).[5,12,27] The strong ionization and solubility properties of 5-FU in the basic conditions promote the release characteristics of its ions from Mg·HAP and β-CD/HAP at pH 7.4 (intestinal fluid) as compared to pH 1.2 (gastric fluid).

However, the ionization behavior of 5-FU induces its release and diffusion properties at the basic conditions, the release profiles of 5-FU from Mg·HAP displays faster properties at pH 1.2 (in gastric fluid) rather than pH 7.4 (in intestinal fluid).[14,17] This behavior was assigned to the low stability and significant degradation properties of the hydroxyapatite structure at the acidic conditions that prompt the notable high release properties from Mg·HAP at pH 1.2. The experimental 5-FU release profiles of Mg·HAP either at the gastric or intestinal fluid extended to more than 60 h (Figure 6A). About 50% of the entrapped quantities of the 5-FU molecules were diffused from Mg·HAP after 14 and 30 h at pH 1.2 and pH 7.4, respectively. The complete 5-FU release states in the gastric and intestinal fluids were detected after about 70 h and nearly 100 h, respectively.

Regarding the 5-FU release profiles of β-CD/HAP, it shows reversible behaviors as compared to the reported release properties of 5-Fu at the different pH conditions. The integration of β-CD resulted in a reduction in the release properties at the acidic environments (pH 1.2) and accelerates notably the release rates at the basic environments (pH 7.4) (Figure 6B). This behavior signifies the significant enhancement effect of the coating surface of β-CD on the stability of the Mg·HAP at acidic conditions and reduces the degradability rate of its structure. Generally, the integration of β-CD resulted in considerably reducing the releaser properties of 5-FU in the gastric fluid (pH 1.2) and a remarkable increase in the release speed at the intestinal fluid (pH 7.4). About 50% of the entrapped quantities of the 5-FU molecules were diffused from β-CD/HAP after 22 and 14 h at pH 1.2 and pH 7.4, respectively. The complete diffusion state within the gastric

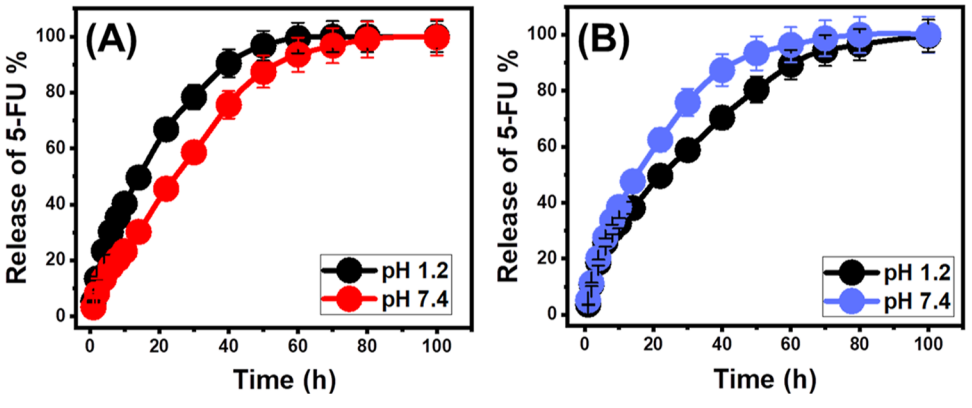

Figure 6. In vitro release profiles of 5-FU from Mg·HAP (A) and β-CD/HAP (B) at pH 1.2 and pH 7.4.

https://doi.org/10.1021/acsomega.3c02982
ACS Omega 2023, 8, 30247−30261

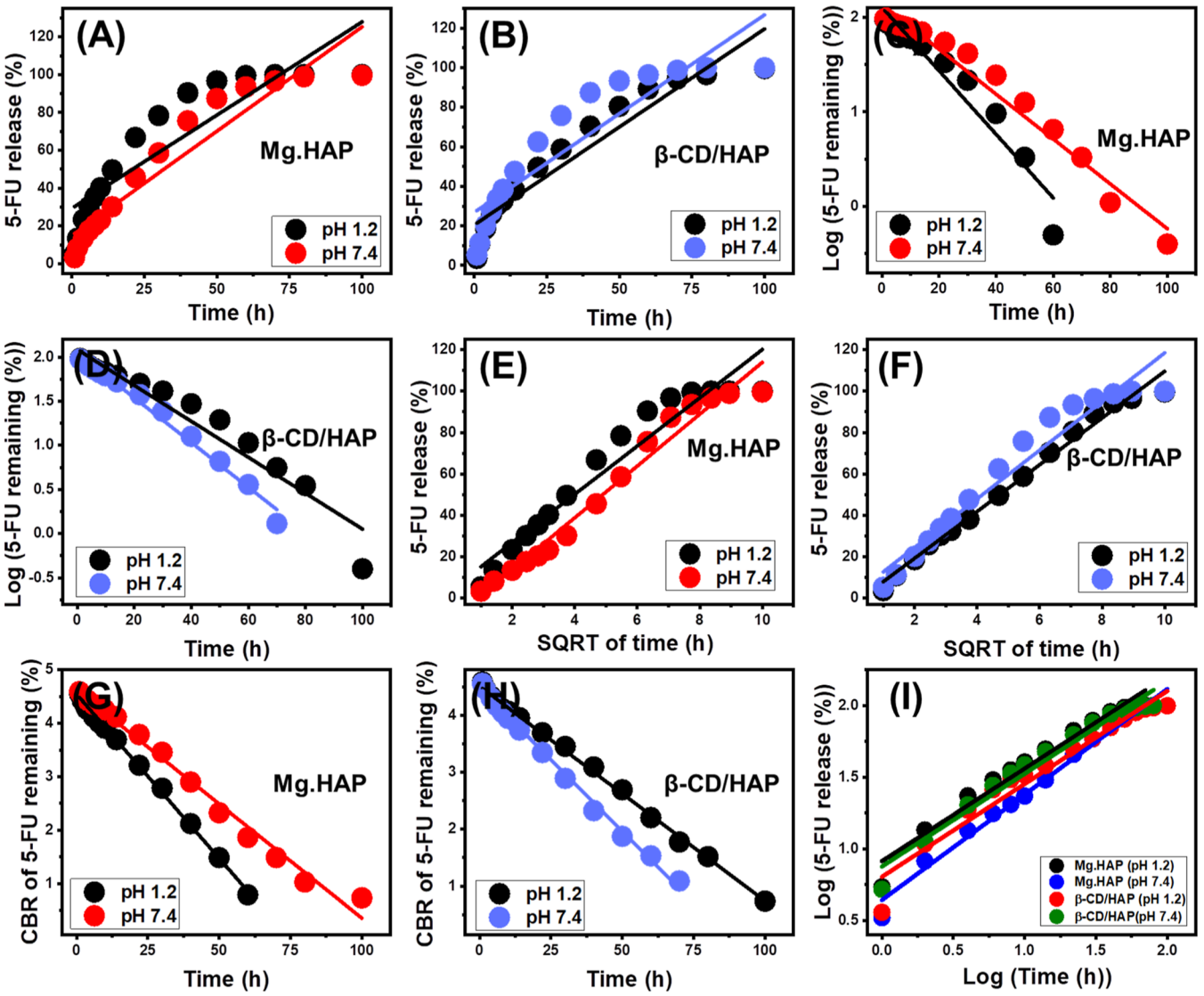

Figure 7. Linear fitting of the detected 5-FU release results with the hypotheses of zero-order (A,B), first-order (C,D), Higuchi (E,F), Hixson–Crowell (G,H), and Korsmeyer–Peppas (I) release kinetic models.

fluid was distinguished after nearly 100 h, while in the intestinal fluid, the maximum diffusion was obtained after 80 h.

In specific situations during which there is a need for prolonged contact and interaction between the medication ions and the cancerous cells, the gradual and regulated diffusion of 5-Fu as an anticancer medication was advised.[5,6] Additionally, in certain situations requiring specific therapeutic doses to be administered within a short period of time, abrupt and quick delivery methods are recommended. As a result, the synthetic β-CD/HAP as prospective carrier of 5-FU may offer a favorable delivery system with regulated encapsulation and release features.

2.4. Release Kinetic Studies. Kinetic analyses of the 5-F release activities from Mg·HAP and β-CD/HAP were carried out as markers of the appropriately regulated mechanistic processes. The kinetic modeling of the release reactions was performed based on the assumption of zero-order (Z-O) (eq 11), first-order (F-O) (eq 12), Higuchi (H-G) (eq 13), Hixson–Crowell (H–C) (eq 14), and Korsmeyer–Peppas (K–P) (eq 15) based on the linear regression fitting levels with these investigated models.[5]

$$W_t - W_0 = K_0 \cdot t \tag{10}$$

$$\ln(W_\infty / W_t) = K_1 \cdot t \tag{11}$$

$$W_t = K_h t^{1/2} \tag{12}$$

$$W_0^{1/3} - W_t^{1/3} = K_{HC} t \tag{13}$$

$$W_t / W_\infty = K_p t^n \tag{14}$$

According to the zero-order kinetics, the release activities of 5-FU from Mg·HAP and β-CD/HAP occur at steady rates and the loading doses having no discernible impact on the behavior.[4] With regard to F-O kinetics, the 5-FU-loaded dosages into Mg·HAP and β-CD/HAP show a substantial effect on the efficiency of the release processes.[1] The Higuchi kinetics (H-G) assumes that the diffusion processes have an essential influence on drug release systems.[1,65] The diffusion process, according to the Higuchi hypothesis, was carried out at a steady rate that was slower than the loaded quantity of 5-FU. Additionally, the used carriers must possess sink properties, and their solubilities and swelling characteristics

https://doi.org/10.1021/acsomega.3c02982
ACS Omega 2023, 8, 30247−30261

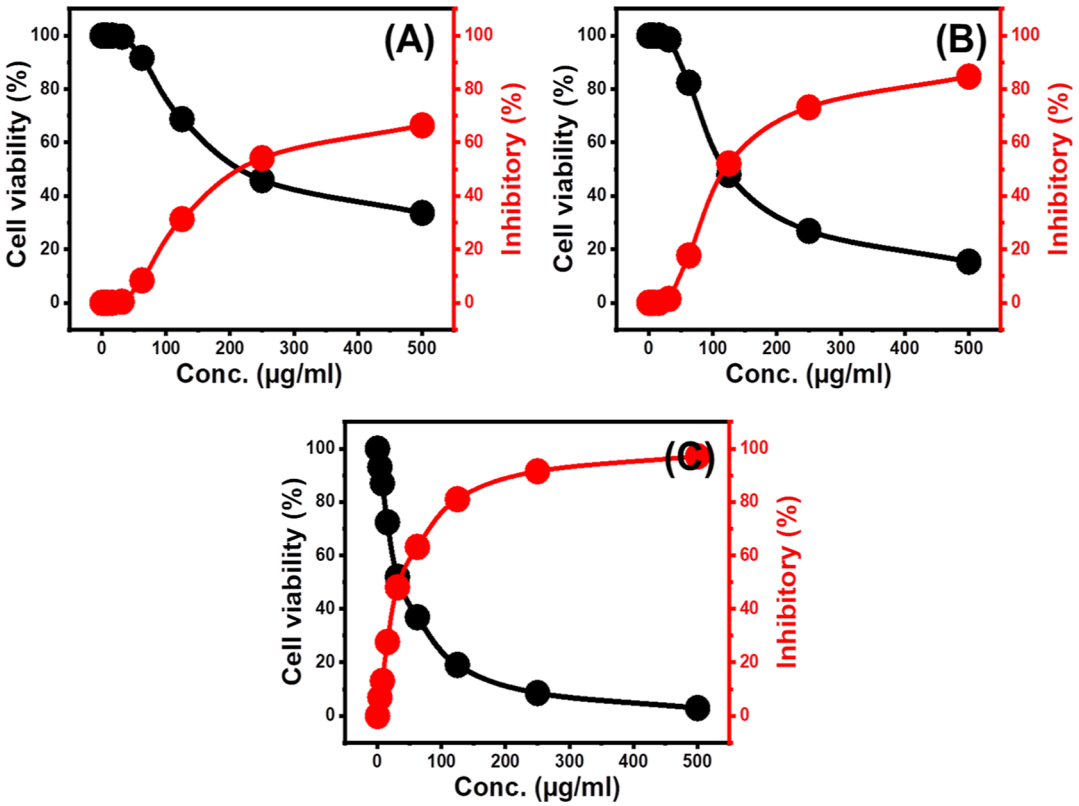

Figure 8. The cytotoxicity effect of free Mg·HAP (A), free β-CD/HAP composite (B), and 5-FU encapsulated β-CD/HAP (C) on colorectal cancer cell (HCT-116).

have an ignored impact on the releasing behaviors.[4] The Hixson−Crowell model's (H−C) supposition relies on erosion mechanisms instead of diffusion, and the efficiency of the erosion reactions depends significantly on the surface area and grain diameter of Mg·HAP and β-CD/HAP.[4,66] With regard to the mechanistic hypothesis of Korsmeyer−Peppas kinetics, the release implies a combination of diffusion and erosion processes.[1,66]

According to the coefficients of determination (R^2), the documented 5-FU release from Mg·HAP and β-CD/HAP more closely corresponds to the properties of the F-O kinetic (Figure 7C,D; Table 1) as compared to the Z-O kinetic (Figure 7A,B; Table 1). This finding suggests that the loaded 5-FU amounts have a significant influence on the efficacy of their release from their host carriers. Excellent agreement between the release processes and both Higuchi (H-G) (Figure 7E,F; Table 1) and Hixson−Crowell (H−C) (Figure 7G,H; Table 1) models was verified by the determined fitting degrees. These kinetic evaluation findings revealed that throughout the 5-FU release activities, diffusion and erosion mechanisms cooperated together. However, the release profiles of both Mg·HAP and β-CD/HAP slightly follow the Hixson−Crowell kinetics at a higher degree and are affected essentially by the erosion mechanisms. This mechanistic hypothesis was reinforced by the substantial fitting levels with the evaluated Korsmeyer−Peppas and expected values of the diffusion exponent (n), which were obtained as a fitting parameter (Figure 7I; Table 1). The values of n are greater than 0.45, verifying the non-Fickian transportation characteristics of the released 5-Fu ions from Mg·HAP and β-CD/HAP as investigated carriers.[47]

2.5. Cytotoxicity Properties. Free Mg·HAP and β-CD/HAP particulate cytotoxicity against healthy colorectal fibroblast cells (CCD-18Co) has been established as one of the key factors for assessing the degree of biocompatibility as well as the safety of the examined materials on healthy and uninfected cells. Also, the human colorectal tumor cell lines (HCT-116) were used to test the cytotoxicity of unloaded β-CD/HAP particulates besides their 5-FU-loaded products to assess their potential as a cancer inhibitor and as a carrier of improved influence on the curative properties of the loaded 5-FU medicine. In terms of the cytotoxic impact of unloaded β-CD/HAP particulates on CCD-18Co cells, the studied composite particulates exhibit excellent biocompatibility and safety on normal cells throughout the assessed doses (20 to 120 g/L). After treating the CCD-18Co cells using the maximum studied dose of unloaded Mg·HAP and β-CD/HAP particulates (120 g/L), the resulting cell viability % are 92.3 and 90.6%, respectively.

Concerning the cytotoxic properties of free Mg·HAP and -CD/HAP particulates on the HCT-116 cancer cells, the synthesized materials as unloaded particulates exhibit notable cytotoxicity toward malignant cells, particularly at doses greater than 50 g/mL (Figure 8). In the presence of 500 g/mL of the unloaded Mg·HAP particulates, the determined cell viability %, inhibition %, and IC_{50} are 33.62%, 66.38%, and 157.18 μg/mL, respectively (Figure 8A) while the reported values of free β-CD/HAP is 15.32% (cell viability), 84.6% (inhibitory %), and 118.7 μg/mL (IC-50 value) (Figure 8B). Such cytotoxic results validate that the promising biological activity of Mg·HAP is enhanced at a considerable rate after its integration with β-CD (β-CD/HAP). Regarding the cytotoxic properties of 5-FU-encapsulated β-CD/HAP, the treatment of the cell lines with

https://doi.org/10.1021/acsomega.3c02982
ACS Omega 2023, 8, 30247−30261

500 μg/mL of it resulted in 2.91% as cell viability percentage, 97.1% as an inhibitory %, and 35.34 μg/mL as IC-50 (Figure 8C). Such cytotoxic findings show, besides its previously established regulating consequences for the loading and release actions, the significant enhanced influence of the utilized β-CD/HAP carrier on cytotoxic responses and the therapeutic value of the supplemented 5-FU medicine on typical chemotherapy.

3. CONCLUSIONS

Synthetic magnesium-doped hydroxyapatite (Mg·HAP) was integrated into a composite with β-CD forming an innovative structure (β-CD/HAP) that has been characterized as a prospective drug carrier for 5-fluorouracil (5-FU) chemotherapy with multifunctional chemical groups. β-CD/HAP exhibits enhanced 5-FU encapsulation properties (272.3 mg/g) than Mg·HAP (164.9 mg/g). This behavior was assigned to the detectable improvement in the surface area and organic affinity in addition to the reactive active site density [61.2 mg/g (β-CD/HAP) and 42.4 mg/g (Mg·HAP)]. The loading behavior of 5-FU into β-CD/HAP involved the adsorption of about 5 molecules per site, and this occurred by physical mechanisms based on the estimated loading energy (<40 kJ/mol). The release profile of β-CD/HAP displays regulated and slow characteristics for a period exceeding 100 h. This resulted as a result of triggered erosion/diffusion processes following release kinetics modeling as well as a diffusion exponent (>0.45). The cell viability of cancer HCT-116 cell lines after their treatment with free β-CD/HAP (33.62%) and 5-FU-loaded products (2.91%) reflected strong inhibition effects on the cancer cells.

4. EXPERIMENTAL WORK

4.1. Materials. The phosphorite precursor [P_2O_5 (28 wt %), CaO (46 wt %), Fe_2O_3 (2 wt %), SiO_2 (12 wt %), Al_2O_3 (0.8 wt %), F (2.8 wt %), Na_2O (4 wt %), MgO (0.5 wt %), and LOI (7 wt %)] were delivered from the Quseir area, Red Sea, Egypt. Magnesium nitrate hexahydrate (99% purity; Sigma-Aldrich, Egypt) was applied as the doped magnesium ions. Nitric acid (40% purity; Sigma-Aldrich, Egypt) and ammonium hydroxide (25% NH_3; Sigma-Aldrich, Egypt) were used during the dissolving/precipitation steps. The β-cyclodextrin (MW 1153 g/mol; >85% purity; Sigma-Aldrich) in addition to ethanol (95%; Sigma-Aldrich) were incorporated as the essential chemicals during the synthesis of the composite with of hydroxyapatite. 5-Fluorouracil drug (analytical grade >99%) obtained from Sigma-Aldrich company; Egypt.

4.2. Synthesis of Magnesium Hydroxyapatite. The fabrication of Mg·HAP was accomplished based on the reported dissolution−precipitation method by Okasha et al.[40] The phosphorite raw samples first were ground to be within the size range of 25−150 μm. Then, the ground product (15 g) was dissolved completely in nitric acid (200 mL; 1 M) over 24 h at 343 K by a magnetic stirrer at an adjusted speed of 200 rpm. The residual solids were removed by filtration utilizing Whatman filter paper (40 μm) remaining solution of Ca^{2+} and PO_4^{3-} ions. Afterward, the magnesium nitrate salt (10 g) was dissolved within the filtered solution under stirring for 2 h. Then the ammonium solution (25% NH_3) was added to the mixture at a slow rate unit for the successful precipitation of the white gel of Mg·HAP. After that, the synthesis system was left at room temperature for 24 h, and then the Mg·HAP product was extracted by another cycle of filtration. Finally, the synthetic Mg·HAP particles were washed for five runs and dried for 10 h at 373 K in an electric muffle furnace to be incorporated into the additional synthesis and application procedures.

4.3. Synthesis of β-Cyclodextrin/Mg·Hydroxyapatite Composite (β-CD/HAP). The synthetic procedures for the β-CD/HAP composite were carried out using the technique described by Altoom et al.[11] A slurry-like mixture was produced by dispersing and homogenizing the β-cyclodextrin powder (1 g) in approximately 80 mL of alcohol for 3 h using a magnetic stirring device (1000 rpm). As part of a cooperative experiment, 2 g of previously produced HAP nanoparticles were subsequently homogenized and pulverized for 60 min in 100 mL of distilled water while being stirred at 1000 rpm and sonicated at 240 W. Afterward, the HAP suspension that had been developed and the β-cyclodextrin slurry were blended together, and the mixture's homogenization occurred by stirring (at 1000 rpm) for 24 h. Then, the mixture was homogenized once again for 24 h using an ultrasound source (240 W), and the resulting composite particulates were separated from it using Whatman filter paper (40 μm). The composite fractions were then washed and dried at 60 °C for 12 h before being used in the subsequent experimental stages. This was done to neutralize the outer surface of the produced β-CD/HAP.

4.4. Analytical Techniques. The degree of crystallinity and the present crystal phases have been measured employing a PANalytical-Empyrean X-ray diffractometer over a detection range of 0 to 70° based on the resulting XRD patterns. The chemical structures of Mg·HAP and β-CD/HAP were distinguished using a Fourier transform infrared spectrometer (FTIR8400S; Shimadzu) within the detection frequency spectrum from 400 to 4000 cm^{-1}. SEM photos were obtained using a scanning electron microscope (Gemini, Zeiss Ultra 55) immediately after coating Mg·HAP and β-CD/HAP with thin gold layers. The predicted changes in the morphological properties of zeolite after the two different modification steps have been confirmed using the obtained SEM images. Additionally, the inner characteristics of Mg·HAP and β-CD/HAP have been studied utilizing the HRTEM images, which were obtained by a transmission electron microscope (JEOL-JEM2100) at an accelerating voltage of 200 kV. The surface area and porosity of Mg·HAP and β-CD/HAP were determined using a surface area analyzer (Beckman Coulter SA3100) and the related N_2 adsorption/desorption isotherms.

4.5. 5-FU Encapsulation Studies. The encapsulating investigations of 5-FU into Mg·HAP and β-CD/HAP were assessed based on the essentially addressed aspects to regulate the 5-FU encapsulated dose as well as its greatest encapsulation capacities. The pH (3−11), encapsulation time (1−14 h), 5-Fu concentration (50−400 mg/L), and temperature (20−60 °C) are the main parameters that were evaluated during the study. The Mg·HAP and β-CD/HAP particles were efficiently homogenized inside the tested 5-FU aqueous solutions (50 mL) by a vortex rotator. Following each test's equilibration duration, the Mg·HAP and β-CD/HAP particles were extracted from the 5-FU solutions by filtering them via Whatman paper, and the remaining 5-FU concentrations were then determined using a UV−vis spectrophotometer at an adjusted wavelength ($\lambda_{(max)}$ = 266 nm). These remaining 5-Fu concentrations have been employed to compute the loading capacities of Mg·HAP and β-CD/HAP in mg/g based on eq

https://doi.org/10.1021/acsomega.3c02982
ACS Omega 2023, 8, 30247−30261

15. The 5-FU loading experiments into Mg·HAP and β-CD/HAP were triplicated, and the calculated average values were provided in the research data with standard deviations of <5.1%.

$$\text{Loaded drug (mg/g)} = \frac{(\text{initial concentration} - \text{residual concentration}) \times \text{solvent volume}}{\text{carrier weight}} \quad (15)$$

4.6. Release Studies. The 5-FU release patterns of Mg·HAP and β-CD/HAP materials were assessed in two different chemical buffers (gastric fluid, pH 1.2, and intestinal fluid, pH 7.4) at 37.5 °C. The 5-FU-loaded Mg·HAP and β-CD/HAP particles (100 mg/g) were extensively dispersed individually throughout 500 mL of the evaluated release buffers. The DISTEK dissolving apparatus homogenized the 5-Fu-loaded Mg·HAP and β-CD/HAP particles and the two distinct buffers for 120 h at 200 rpm as the adjusted vessel's rotational speed. To monitor the 5-FU diffusion percentages from Mg·HAP and β-CD/HAP, a UV−vis spectrophotometer was employed to analyze samples of the two different buffered solutions (5 mL), which were taken at periodic intervals from the bulk volumes of the release solutions. The bulk release buffers were immediately replenished with the regularly collected samples to keep the volumes at exactly the same levels during the entire release time. The 5-FU release experiments were completed in triplicate, and the calculated average results were given in the studies using eq 16 with a standard deviation of less than 4.16%.

$$\text{Drug release (\%)} = \frac{\text{the amount of released 5-Fu}}{\text{amount of loaded 5-Fu}} \times 100 \quad (16)$$

4.7. In Vitro Cytotoxicity. *4.7.1. Cell Lines.* Colorectal cancer cell lines (HCT-116) were delivered from the American Type Culture Collection (ATCC, Rockville, MD) and assessed as the target cancer cells during the conducted cytotoxic assays. Gentamycin, 0.25% trypsin−EDTA, fetal bovine serum, HEPES buffer, dimethyl sulfoxide (DMSO), RPMI-1640, 3-(4,5-dimethylthiazol-2-yl)-2,5-diphenyltetrazolium bromide (MTT 99%), and DMEM are the essential chemical reagents that were employed during the performed incubation process and cytotoxic assays.

4.7.2. In Vitro Cytotoxicity. RPMI-1640 medium combined with 50 g/mL gentamycin and 10% fetal calf serum was first used to cultivate the malignant HCT-116 cell lines at 37 °C and 5% CO_2. The malignant cell lines (5×10^4 cells/well) had been cultured for three weeks before being immersed in Corning-96-well plates for 24 h. Then, particular dosages of the 5-FU-loaded Mg·HAP and β-CD/HAP were administered to the cell strains that were then cultured for further 24 h. The number of viable cells generated throughout the duration of incubation was determined using the widely employed MTT cell proliferation assessment. The incorporated culture medium was efficiently removed by finishing the incubation cycle and replaced with newly generated media (100 μL of RPMI). The freshly added media was mixed thoroughly with the MTT (10 μL; 12 mM), and the combination was then cultured once more for 5 h to see whether formazan with a distinguishable purple hue had grown. The generated formazan was then successfully dissolved using 50 μL of DMSO solution. In the last stage, a microplate set to a particular wavelength of 590 nm is used to measure the optical densities (ODs) of the cell lines that were cultivated during the investigations. According to eq 17, the computed values were utilized to determine the cell viability percentage.

$$\text{Cell viability (\%)} = \frac{\text{mean OD}}{\text{control OD}} \times 100 \quad (17)$$

AUTHOR INFORMATION

Corresponding Author

Mostafa R. Abukhadra − *Materials Technologies and Their Applications Lab, Geology Department, Faculty of Science and Geology Department, Faculty of Science, Beni-Suef University, Beni Suef City 62511, Egypt;* orcid.org/0000-0001-5404-7996; Email: Abukhadra89@Science.bsu.edu.eg

Authors

Alaa T. Okasha − *Materials Technologies and Their Applications Lab, Geology Department, Faculty of Science, Beni-Suef University, Beni Suef City 62511, Egypt; Department of Chemistry, Faculty of Science, Beni-Suef University, Beni Suef City 62514, Egypt*

Sarah I. Al Othman − *Princess Nourah bint Abdulrahman University, College of Science, Biology Department, Riyadh, Saudi Arabia*

Haifa E. Alfassam − *Princess Nourah bint Abdulrahman University, College of Science, Biology Department, Riyadh, Saudi Arabia*

Noof A. Alenazi − *Department of Chemistry, College of Science and Humanities in Al-Kharj, Prince Sattam Bin Abdulaziz University, Al-Kharj 11942, Saudi Arabia*

Ali A. AlHammadi − *Chemical Engineering Department, Khalifa University of Science and Technology, Abu Dhabi 127788, United Arab Emirates; Center for Catalysis and Separations, Khalifa University, Abu Dhabi 127788, United Arab Emirates*

Ahmed A. Allam − *Zoology Department, Faculty of Science, Beni-Suef University, Beni-Suef 62511, Egypt*

Complete contact information is available at: https://pubs.acs.org/10.1021/acsomega.3c02982

Author Contributions

This article was written through the contributions of all authors. All authors have given approval to the final version of the manuscript.

Notes

The authors declare no competing financial interest.

ACKNOWLEDGMENTS

The authors acknowledge Princess Nourah bint Abdulrahman University Researchers Supporting Project number (PNURSP2023R400), Princess Nourah bint Abdulrahman University, Riyadh, Saudi Arabia.

REFERENCES

(1) El-Zeiny, H. M.; Abukhadra, M. R.; Sayed, O. M.; Osman, A. H. M.; Ahmed, S. A. Insight into Novel β-Cyclodextrin-Grafted-Poly (N-Vinylcaprolactam) Nanogel Structures as Advanced Carriers for 5-Fluorouracil: Equilibrium Behavior and Pharmacokinetic Modeling. *Colloids Surf., A* **2020**, *586*, 124197.

(2) Cutrim, E. S. M.; Vale, A. A. M.; Manzani, D.; Barud, H. S.; Rodríguez-Castellón, E.; Santos, A. P. S. A.; Alcântara, A. C. S. Preparation, Characterization and in Vitro Anticancer Performance of

Nanoconjugate Based on Carbon Quantum Dots and 5-Fluorouracil. *Mater. Sci. Eng. C* **2021**, *120*, 111781.
(3) Abuzar, S. M.; Park, E. J.; Seo, Y.; Lee, J.; Baik, S. H.; Hwang, S.-J. Preparation and Evaluation of Intraperitoneal Long-Acting Oxaliplatin-Loaded Multi-Vesicular Liposomal Depot for Colorectal Cancer Treatment. *Pharmaceutics* **2020**, *12*, 736.
(4) Othman, S. I.; Allam, A. A.; Al Fassam, H.; Abu-Taweel, G. M.; Altoom, N.; Abukhadra, M. R. Sonoco Green Decoration of Clinoptilolite with MgO Nanoparticles as a Potential Carrier for 5-Fluorouracil Drug: Loading Behavior, Release Profile, and Cytotoxicity. *J. Inorg. Organomet. Polym. Mater.* **2021**, *31*, 4608−4622.
(5) Tian, L.; Abukhadra, M. R.; Mohamed, A. S.; Nadeem, A.; Ahmad, S. F.; Ibrahim, K. E. Insight into the Loading and Release Properties of an Exfoliated Kaolinite/Cellulose Fiber (EXK/CF) Composite as a Carrier for Oxaliplatin Drug: Cytotoxicity and Release Kinetics. *ACS Omega* **2020**, *5*, 19165−19173.
(6) Sundaramoorthy, P.; Ramasamy, T.; Mishra, S. K.; Jeong, K.-Y.; Yong, C. S.; Kim, J. O.; Kim, H. M. Engineering of Caveolae-Specific Self-Micellizing Anticancer Lipid Nanoparticles to Enhance the Chemotherapeutic Efficacy of Oxaliplatin in Colorectal Cancer Cells. *Acta Biomater.* **2016**, *42*, 220−231.
(7) Praphakar, R. A.; Jeyaraj, M.; Mehnath, S.; Higuchi, A.; Ponnamma, D.; Sadasivuni, K. K.; Rajan, M. A pH-Sensitive Guar Gum-Grafted-Lysine-β-Cyclodextrin Drug Carrier for the Controlled Release of 5-Flourouracil into Cancer Cells. *J. Mater. Chem. B* **2018**, *6*, 1519−1530.
(8) Lee, J. E.; Abuzar, S. M.; Seo, Y.; Han, H.; Jeon, Y.; Park, E. J.; Baik, S. H.; Hwang, S.-J. Oxaliplatin-Loaded Chemically Cross-Linked Hydrogels for Prevention of Postoperative Abdominal Adhesion and Colorectal Cancer Therapy. *Int. J. Pharm.* **2019**, *565*, 50−58.
(9) Itoo, A. M.; Paul, M.; Ghosh, B.; Biswas, S. Oxaliplatin Delivery via Chitosan/Vitamin E Conjugate Micelles for Improved Efficacy and MDR-Reversal in Breast Cancer. *Carbohydr. Polym.* **2022**, *282*, 119108.
(10) Li, Y.; Sun, Z.; Cui, Y.; Zhang, H.; Zhang, S.; Wang, X.; Liu, S.; Gao, Q. Oxaliplatin Derived Monofunctional Triazole-Containing Platinum(II) Complex Counteracts Oxaliplatin-Induced Drug Resistance in Colorectal Cancer. *Bioorg. Chem.* **2021**, *107*, 104636.
(11) Altoom, N.; Ibrahim, S. M.; Othman, S. I.; Allam, A. A.; Alqhtani, H. A.; Al-Otaibi, F. S.; Abukhadra, M. R. Characterization of β-Cyclodextrin/Phillipsite (β-CD/Ph) Composite as a Potential Carrier for Oxaliplatin as Therapy for Colorectal Cancer; Loading, Release, and Cytotoxicity. *Colloids Surf., A* **2022**, *648*, 129144.
(12) Sayed, M. A.; El-Zeiny, H. M.; Khim, J. S.; Ajarem, J. S.; Allam, A. A.; Abukhadra, M. R. Insight into the Loading Properties of Na+ Green-Functionalized Clinoptilolite as a Potential Carrier for the 5-Fluorouracil Drug, Its Release Kinetics, and Cytotoxicity. *ACS Omega* **2022**, *7*, 6991−7001.
(13) Tan, D.; Yuan, P.; Dong, F.; He, H.; Sun, S.; Liu, Z. Selective Loading of 5-Fluorouracil in the Interlayer Space of Methoxy-Modified Kaolinite for Controlled Release. *Appl. Clay Sci.* **2018**, *159*, 102−106.
(14) Abukhadra, M. R.; Refay, N. M.; El-Sherbeeny, A. M.; El-Meligy, M. A. Insight into the Loading and Release Properties of MCM-48/Biopolymer Composites as Carriers for 5-Fluorouracil: Equilibrium Modeling and Pharmacokinetic Studies. *ACS Omega* **2020**, *5*, 11745−11755.
(15) Çiftçi, H.; Arpa, M. D.; Gülaçar, İ. M.; Özcan, L.; Ersoy, B. Development and Evaluation of Mesoporous Montmorillonite/Magnetite Nanocomposites Loaded with 5-Fluorouracil. *Microporous Mesoporous Mater.* **2020**, *303*, 110253.
(16) Elsayed, E. W.; El-Ashmawy, A. A.; El-Bassyouni, G. T.; Mousa, S. M.; El-Manawaty, M.; Emara, L. H. Formulation and Evaluation of Alginate-Gelatin Hydrogel Scaffolds Loaded with Zinc-Doped Hydroxyapatite and 5-Fluorouracil. *Int. J. Biol. Macromol.* **2023**, *237*, 124147.
(17) Manikantan, V.; Sri Varalakshmi, G.; Sumohan Pillai, A.; Alexander, A.; Lucas, A.; Kathiravan, E.; Allben Akash, B.; V M V Enoch, I. 5-Fluorouracil-Loaded Designed Praseodymium Oxide − Poly- β-Cyclodextrin Nanorods for Effectively Inhibiting Breast Cancer Cells. *Inorg. Chem. Commun.* **2023**, *153*, 110830.
(18) Shad, P. M.; Karizi, S. Z.; Javan, R. S.; Mirzaie, A.; Noorbazargan, H.; Akbarzadeh, I.; Rezaie, H. Folate Conjugated Hyaluronic Acid Coated Alginate Nanogels Encapsulated Oxaliplatin Enhance Antitumor and Apoptosis Efficacy on Colorectal Cancer Cells (HT29 Cell Line). *Toxicol. in Vitro* **2020**, *65*, 104756.
(19) Luo, H.; Ji, D.; Li, C.; Zhu, Y.; Xiong, G.; Wan, Y. Layered Nanohydroxyapatite as a Novel Nanocarrier for Controlled Delivery of 5-Fluorouracil. *Int. J. Pharm.* **2016**, *513*, 17−25.
(20) Khang, M. K.; Zhou, J.; Co, C. M.; Li, S.; Tang, L. A Pretargeting Nanoplatform for Imaging and Enhancing Anti-Inflammatory Drug Delivery. *Bioact. Mater.* **2020**, *5*, 1102−1112.
(21) Rahbar, M.; Morsali, A.; Bozorgmehr, M. R.; Beyramabadi, S. A. Quantum Chemical Studies of Chitosan Nanoparticles as Effective Drug Delivery Systems for 5-Fluorouracil Anticancer Drug. *J. Mol. Liq.* **2020**, *302*, 112495.
(22) Wan, Y.; Cui, T.; Xiong, G.; Li, W.; Tu, J.; Zhu, Y.; Luo, H. Magnetic Lamellar Nanohydroxyapatite as a Novel Nanocarrier for Controlled Delivery of 5-Fluorouracil. *Ceram. Int.* **2017**, *43*, 4957−4964.
(23) Ramasamy, S.; Dhamecha, D.; Kaliyamoorthi, K.; Pillai, A. S.; Alexander, A.; Dhanaraj, P.; Menon, J. U.; Enoch, I. V. M. V. Magnetic Hydroxyapatite Nanomaterial−Cyclodextrin Tethered Polymer Hybrids as Anticancer Drug Carriers. *Mater. Adv.* **2021**, *2*, 3315−3327.
(24) Cai, A.; Zhu, Y.; Qi, C. Biodegradable Inorganic Nanostructured Biomaterials for Drug Delivery. *Adv. Mater. Interfaces* **2020**, *7*, 2000819.
(25) Huang, S.-M.; Liu, S.-M.; Ko, C.-L.; Chen, W.-C. Advances of Hydroxyapatite Hybrid Organic Composite Used as Drug or Protein Carriers for Biomedical Applications: A Review. *Polymers* **2022**, *14*, 976.
(26) Sayed, I. R.; Farhan, A. M.; AlHammadi, A. A.; El-Sayed, M. I.; Abd El-Gaied, I. M.; El-Sherbeeny, A. M.; Al Zoubi, W.; Ko, Y. G.; Abukhadra, M. R. Synthesis of Novel Nanoporous Zinc Phosphate/Hydroxyapatite Nano-Rods (ZPh/HPANRs) Core/Shell for Enhanced Adsorption of Ni^{2+} and Co^{2+} Ions: Characterization and Application. *J. Mol. Liq.* **2022**, *360*, 119527.
(27) Ofudje, E. A.; Adedapo, A. E.; Oladeji, O. B.; Sodiya, E. F.; Ibadin, F. H.; Zhang, D. Nano-Rod Hydroxyapatite for the Uptake of Nickel Ions: Effect of Sintering Behaviour on Adsorption Parameters. *J. Environ. Chem. Eng.* **2021**, *9*, 105931.
(28) Pai, S.; Kini, M. S.; Mythili, R.; Selvaraj, R. Adsorptive Removal of AB113 Dye Using Green Synthesized Hydroxyapatite/Magnetite Nanocomposite. *Environ. Res.* **2022**, *210*, 112951.
(29) Barbosa, A. A.; Júnior, S. A.; Mendes, R. L.; de Lima, R. S.; de Vasconcelos Ferraz, A. Multifunctional Hydroxyapatite with Potential for Application in Theranostic Nanomedicine. *Mater. Sci. Eng. C* **2020**, *116*, 111227.
(30) Pujari-Palmer, S.; Chen, S.; Rubino, S.; Weng, H.; Xia, W.; Engqvist, H.; Tang, L.; Ott, M. K. In vivo and in vitro evaluation of hydroxyapatite nanoparticle morphology on the acute inflammatory response. *Biomaterials* **2016**, *90*, 1−11.
(31) Tran, T. N.; Do, Q. C.; Kim, D.; Kim, J.; Kang, S. Urchin-like Structured Magnetic Hydroxyapatite for the Selective Separation of Cerium Ions from Aqueous Solutions. *J. Hazard. Mater.* **2022**, *430*, 128488.
(32) Fan, L.; Kong, W.; Gao, C.; Zhu, P. Synthesis of Highly Porous Iron-Doped Carbonated Hydroxyapatite Spheres for Efficient Adsorption of Carmine Dyes. *SSRN Electron. J.* **2021**, *20*, 101205.
(33) Mossavi, E.; Hosseini Sabzevari, M.; Ghaedi, M.; Ahmadi Azqhandi, M. H. Adsorption of the Azo Dyes from Wastewater Media by a Renewable Nanocomposite Based on the Graphene Sheets and Hydroxyapatite/ZnO Nanoparticles. *J. Mol. Liq.* **2022**, *350*, 118568.
(34) Akash, B. A.; Kanagaraj, S.; Sundaravadivelu, S.; Varalakshmi, G. S.; Manikantan, V.; Pillai, A. S.; Alexander, A.; Enoch, I. V. M. V. Cobalt-Nickel Alloy Nanoparticles Surface-Functionalized with

https://doi.org/10.1021/acsomega.3c02982
ACS Omega 2023, 8, 30247−30261

Cyclodextrin for Delivering 5-Fluorouracil. *J. Mol. Struct.* **2023**, *1290*, 135906.
(35) Krawczyk, K.; Silvestri, D.; Nguyen, N. H. A.; Ševců, A.; Łukowiec, D.; Padil, V. V. T.; Řezanka, M.; Černík, M.; Dionysiou, D. D.; Wacławek, S. Enhanced Degradation of Sulfamethoxazole by a Modified Nano Zero-Valent Iron with a β-Cyclodextrin Polymer: Mechanism and Toxicity Evaluation. *Sci. Total Environ.* **2022**, *817*, 152888.
(36) El-Sherbeeny, A. M.; Ibrahim, S. M.; AlHammadi, A. A.; Soliman, A. T. A.; Shim, J.-J.; Abukhadra, M. R. Effective Retention of Radioactive Cs^{+} and Ba^{2+} Ions Using β-Cyclodextrin Functionalized Diatomite (β-CD/D) as Environmental Adsorbent; Characterization, Application, and Safety. *Surf. Interfaces* **2021**, *26*, 101434.
(37) Bandura, L.; Białoszewska, M.; Malinowski, S.; Franus, W. Adsorptive Performance of Fly Ash-Derived Zeolite Modified by β-Cyclodextrin for Ibuprofen, Bisphenol A and Caffeine Removal from Aqueous Solutions − Equilibrium and Kinetic Study. *Appl. Surf. Sci.* **2021**, *562*, 150160.
(38) (a) Jiang, Y.; Abukhadra, M. R.; Refay, N. M.; Sharaf, M. F.; El-Meligy, M. A.; Awwad, E. M. Synthesis of Chitosan/MCM-48 and β-Cyclodextrin/MCM-48 Composites as Bio-Adsorbents for Environmental Removal of Cd^{2+} Ions; Kinetic and Equilibrium Studies. *React. Funct. Polym.* **2020**, *154*, 104675. (b) Bin Jumah, M. N.; Eid, M. H.; AL-Huqail, A. A.; Mohammad, M. A.; Bin-Murdhi, N. S.; Abu-Taweel, G. M.; Altoom, N.; Allam, A. A.; AbuKhadra, M. R. . Enhanced Remediation of As (V) and Hg (II) Ions from Aqueous Environments Using β-Cyclodextrin/MCM-48 Composite: Batch and Column Studies. *J. Water Process. Eng.* **2021**, *42*, 102118.
(39) Hariharan, M. S.; Sivaraj, R.; Ponsubha, S.; Jagadeesh, R.; Enoch, I. V. M. V. 5-Fluorouracil-Loaded β-Cyclodextrin-Carrying Polymeric Poly(Methylmethacrylate)-Coated Samarium Ferrite Nanoparticles and Their Anticancer Activity. *J. Mater. Sci.* **2018**, *54*, 4942−4951.
(40) Okasha, A. T.; Abdel-Khalek, A. A.; El-Sherbeeny, A. M.; Zoubi, W. A.; Abukhadra, M. R. Advanced Equilibrium Study on the Synthesis and Characterization of Mg-Doped Hydroxyapatite Nano-Fibers as a Potential Enhanced Adsorbent of Zn (II) and Malachite Green Dye. *Mater. Today Commun.* **2023**, *35*, 105883.
(41) Zhou, Y.; Li, W.; Jiang, X.; Sun, Y.; Yang, H.; Liu, Q.; Cao, Y.; Zhang, Y.; Cheng, H. RETRACTED: Synthesis of Strontium (Sr) Doped Hydroxyapatite (HAp) Nanorods for Enhanced Adsorption of Cr (VI) Ions from Wastewater. *Ceram. Int.* **2021**, *47*, 16730−16736.
(42) Xiong, T.; Li, Q.; Liao, J.; Zhang, Y.; Zhu, W. Highly Enhanced Adsorption Performance to Uranium(VI) by Facile Synthesized Hydroxyapatite Aerogel. *J. Hazard. Mater.* **2022**, *423*, 127184.
(43) Foroutan, R.; Peighambardoust, S. J.; Ahmadi, A.; Akbari, A.; Farjadfard, S.; Ramavandi, B. Adsorption Mercury, Cobalt, and Nickel with a Reclaimable and Magnetic Composite of Hydroxyapatite/Fe3O4/Polydopamine. *J. Environ. Chem. Eng.* **2021**, *9*, 105709.
(44) Mehta, D.; Mondal, P.; Saharan, V. K.; George, S. In-Vitro Synthesis of Marble Apatite as a Novel Adsorbent for Removal of Fluoride Ions from Ground Water: An Ultrasonic Approach. *Ultrason. Sonochem.* **2018**, *40*, 664−674.
(45) Nguyen, P. T.; Nguyen, X. T.; Nguyen, T. V.; Nguyen, T. T.; Vu, T. Q.; Nguyen, H. T.; Pham, N. T.; Thi Dinh, T. M. Treatment of Cd2+ and Cu2+ Ions Using Modified Apatite Ore. *J. Chem.* **2020**, *2020*, 1−12.
(46) Abukhadra, M. R.; Refay, N. M.; El-Sherbeeny, A. M.; Mostafa, A. M.; Elmeligy, M. A. Facile Synthesis of Bentonite/Biopolymer Composites as Low-Cost Carriers for 5-Fluorouracil Drug; Equilibrium Studies and Pharmacokinetic Behavior. *Int. J. Biol. Macromol.* **2019**, *141*, 721−731.
(47) Abdel Salam, M.; Mokhtar, M.; Albukhari, S. M.; Baamer, D. F.; Palmisano, L.; Jaremko, M.; Abukhadra, M. R. Synthesis and Characterization of Green ZnO@polynaniline/Bentonite Tripartite Structure (G.Zn@PN/BE) as Adsorbent for As (V) Ions: Integration, Steric, and Energetic Properties. *Polymers* **2022**, *14*, 2329.
(48) Salam, M. A.; Abukhadra, M. R.; Mostafa, M. Effective Decontamination of As(V), Hg(II), and U(VI) Toxic Ions from Water Using Novel Muscovite/Zeolite Aluminosilicate Composite: Adsorption Behavior and Mechanism. *Environ. Sci. Pollut. Res.* **2020**, *27*, 13247−13260.
(49) El Qada, E. Kinetic Behavior of the Adsorption of Malachite Green UsingJordanian Diatomite as Adsorbent. *Jordanian J. Eng. Chem. Ind.* **2020**, *3*, 1−10.
(50) Lin, X.; Xie, Y.; Lu, H.; Xin, Y.; Altaf, R.; Zhu, S.; Liu, D. Facile Preparation of Dual La-Zr Modified Magnetite Adsorbents for Efficient and Selective Phosphorus Recovery. *Chem. Eng. J.* **2021**, *413*, 127530.
(51) Albukhari, S. M.; Salam, M. A.; Abukhadra, M. R. Effective Retention of Inorganic Selenium Ions (Se (VI) and Se (IV)) Using Novel Sodalite Structures from Muscovite; Characterization and Mechanism. *J. Taiwan Inst. Chem. Eng.* **2021**, *120*, 116−126.
(52) Abukhadra, M. R.; El Kashief, F. A.; Othman, S. I.; Alqhtani, H. A.; Allam, A. A. Synthesis and Characterization of Fe0@chitosan/Cellulose Biocompatible Composites from Natural Resources as Advanced Carriers for Ibuprofen Drug: Reaction Kinetics and Equilibrium. *New J. Chem.* **2022**, *46*, 12797−12807.
(53) Sherlala, A. I. A.; Raman, A. A. A.; Bello, M. M.; Buthiyappan, A. Adsorption of Arsenic Using Chitosan Magnetic Graphene Oxide Nanocomposite. *J. Environ. Manage.* **2019**, *246*, 547−556.
(54) Huang, Y.; Zeng, X.; Guo, L.; Lan, J.; Zhang, L.; Cao, D. Heavy Metal Ion Removal of Wastewater by Zeolite-Imidazolate Frameworks. *Sep. Purif. Technol.* **2018**, *194*, 462−469.
(55) Jasper, E. E.; Ajibola, V. O.; Onwuka, J. C. Nonlinear Regression Analysis of the Sorption of Crystal Violet and Methylene Blue from Aqueous Solutions onto an Agro-Waste Derived Activated Carbon. *Appl. Water Sci.* **2020**, *10*, 132.
(56) Oluchukwu, A.; Maxwell, O.; Albert, A. Equilibrium Isotherm Studies on the Adsorption of Malachite Green and Lead Ion from Aqueous Solution Using Locally Activated Ugwaka Clay (Black Clay). *Arch. Curr. Res. Int.* **2018**, *12*, 1−11.
(57) Yang, X.; Wang, J.; El-Sherbeeny, A. M.; AlHammadi, A. A.; Park, W.-H.; Abukhadra, M. R. Insight into the Adsorption and Oxidation Activity of a ZnO/Piezoelectric Quartz Core-Shell for Enhanced Decontamination of Ibuprofen: Steric, Energetic, and Oxidation Studies. *Chem. Eng. J.* **2022**, *431*, 134312.
(58) Sellaoui, L.; Guedidi, H.; SarraWjihi, S.; Reinert, L.; Knani, S.; Duclaux, L.; Ben Lamine, A. Experimental and Theoretical Studies of Adsorption of Ibuprofen on Raw and Two Chemically Modified Activated Carbons: New Physicochemical Interpretations. *RSC Adv.* **2016**, *6*, 12363−12373.
(59) Ali, R. A. M.; Mobarak, M.; Badawy, A. M.; Lima, E. C.; Seliem, M. K.; Ramadan, H. S. New Insights into the Surface Oxidation Role in Enhancing Congo Red Dye Uptake by Egyptian Ilmenite Ore: Experiments and Physicochemical Interpretations. *Surf. Interfaces* **2021**, *26*, 101316.
(60) Ashraf, M.-T.; AlHammadi, A. A.; El-Sherbeeny, A. M.; Alhammadi, S.; Al Zoubi, W.; Ko, Y. G.; Abukhadra, M. R. Synthesis of Cellulose Fibers/Zeolite-A Nanocomposite as an Environmental Adsorbent for Organic and Inorganic Selenium Ions; Characterization and Advanced Equilibrium Studies. *J. Mol. Liq.* **2022**, *360*, 119573.
(61) AbouAitah, K.; Bil, M.; Pietrzykowska, E.; Szałaj, U.; Fudala, D.; Woźniak, B.; Nasiłowska, J.; Swiderska-Sroda, A.; Lojkowski, M.; Sokołowska, B.; Swieszkowski, W.; Lojkowski, W. Drug-Releasing Antibacterial Coating Made from Nano-Hydroxyapatite Using the Sonocoating Method. *Nanomaterials* **2021**, *11*, 1690.
(62) Wang, J.; Cai, N.; Chan, V.; Zeng, H.; Shi, H.; Xue, Y.; Yu, F. Antimicrobial Hydroxyapatite Reinforced-Polyelectrolyte Complex Nanofibers with Long-Term Controlled Release Activity for Potential Wound Dressing Application. *Colloids Surf., A* **2021**, *624*, 126722.
(63) Mostafa, M.; El-Meligy, M. A.; Sharaf, M.; Soliman, A. T.; AbuKhadra, M. R. Insight into Chitosan/Zeolite-A Nanocomposite as an Advanced Carrier for Levofloxacin and Its Anti-Inflammatory Properties; Loading, Release, and Anti-Inflammatory Studies. *Int. J. Biol. Macromol.* **2021**, *179*, 206−216.
(64) Ge, M.; Tang, W.; Du, M.; Liang, G.; Hu, G.; Jahangir Alam, S. M. Research on 5-Fluorouracil as a Drug Carrier Materials with Its in

https://doi.org/10.1021/acsomega.3c02982
ACS Omega 2023, 8, 30247−30261

Vitro Release Properties on Organic Modified Magadiite. *Eur. J. Pharm. Sci.* **2019**, *130*, 44−53.
(65) Ibrahim, S. M.; Bin Jumah, M. N.; Othman, S. I.; Alruhaimi, R. S.; Al-Khalawi, N.; Salama, Y. F.; Allam, A. A.; Abukhadra, M. R. Synthesis of Chitosan/Diatomite Composite as an Advanced Delivery System for Ibuprofen Drug; Equilibrium Studies and the Release Profile. *ACS Omega* **2021**, *6*, 13406−13416.
(66) El-Hamshary, H.; El-Newehy, M. H.; Moydeen Abdulhameed, M.; El-Faham, A.; Elsherbiny, A. S. Evaluation of Clay-Ionene Nanocomposite Carriers for Controlled Drug Delivery: Synthesis, in Vitro Drug Release, and Kinetics. *Mater. Chem. Phys.* **2019**, *225*, 122−132.

https://doi.org/10.1021/acsomega.3c02982
ACS Omega 2023, 8, 30247−30261